AIAA JOURNAL
Vol. 41, No. 3, March 2003

Noise, Turbulence, and Thrust of Subsonic Freejets from Lobed Nozzles

K. B. M. Q. Zaman,* F. Y. Wang,† and N. J. Georgiadis‡
NASA John H. Glenn Research Center at Lewis Field, Cleveland, Ohio 44135

A study of noise benefit, vis-à-vis thrust penalty, and its correlation to turbulence intensities is conducted for freejets issuing from lobed nozzles. Four convergent nozzles with constant exit area are used in the experiments. Three of these are of rectangular lobed configuration having 6, 10, and 14 lobes; the fourth is a circular nozzle. Increasing the number of lobes results in a progressive reduction in the turbulence intensities as well as in the overall radiated noise. The noise reduction is pronounced at the low-frequency end of the spectrum. However, there is an increase in the high-frequency noise that renders the overall benefit less attractive when compared on a scaled-up A-weighted basis. Increasing the number of lobes involves progressive reduction in the thrust coefficient. The measured thrust loss is shown to be primarily caused by increased amount of low-momentum boundary-layer fluid over the stretched perimeter. It is inferred that a moderate number of lobes effectively reduce the noise, but increasing the number further results in a diminishing noise benefit and a rapidly increasing thrust penalty. An analysis, showing that the loss in thrust coefficient is proportional to the perimeter-to-diameter ratio and the inverse of the square root of the Reynolds number, provides a guideline for the choice of the lobe dimensions.

I. Introduction

THIS experimental investigation was prompted by an earlier study[1] in which far-field noise of high subsonic jets from several rectangular and tabbed nozzles and a lobed nozzle were reported. The six-lobed nozzle exhibited significantly lower noise compared to the other cases. Later, through limited experiments the lobed nozzle was also found to involve remarkably lower turbulence intensities.[2,3] A detailed study of the noise benefit, the corresponding thrust penalty, and its correlation to the structure of the turbulent flowfield was considered a worthy effort. This led to the present investigation.

"Lobed forced mixers" or corrugated splitter plates are often used in the industry in order to achieve efficient mixing between two streams. There have been several studies of a basic two-stream mixing layer originating from such a splitter plate.[4–8] One obvious effect of the lobed geometry is the increase in the interfacial area between the two streams that enhances the mixing. Depending on the geometry, the lobes can also introduce pairs of counter-rotating streamwise vortices that efficiently transport momentum and species across the mixing layer. Cross-stream components of vorticity shed from the trailing edges of the lobes, and their subsequent dynamics, can also play a role in the mixing enhancement.

Many researchers have investigated jet flows from nozzles with lobed exit lips or other modified shapes.[9–15] Faster spreading of the jet was observed in all instances. Furthermore, some reduction in jet noise with the use of lobed nozzles has been observed in some of the cited work as well as in the industry. Unfortunately, because of the complex geometry and large parameter space the underlying flow mechanisms have remained far from being completely understood. The processes that impact the noise field of these nozzles are even less understood at this time. It is apparent that further model-scale experiments would be helpful for advancing the understanding and providing a database for developing engineering correlations for the prediction of mixing and noise. It is with this spirit that the present investigation was initiated. The objective has been to measure the flow and noise fields in detail for a systematic parametric variation.

However, because of the many parameters, for example, shape, size, spacing, and distribution of the lobes, only limited variation was possible. The goal was set to examine the effect of the number of lobes for a fixed exit area of the nozzle. The nozzles were convergent, and the flow exited parallel in all cases. Thus, there was no intentional generation of streamwise vorticity, as done in some geometries by "vectoring" the flow from alternate lobes. All experiments were conducted for "cold" freejets. All acoustic data were taken at a high subsonic Mach number ($M_j = 0.94$) to allow reliable noise measurement while avoiding shock-associated complications. The flow surveys at that condition, on the other hand, had to be limited because of inherent measurement difficulty in compressible flows. Nevertheless, after demonstrating that the centerline velocity and turbulence profiles at the high (0.94) and a low (0.30) Mach number were essentially similar further flowfield measurement was conducted at the latter condition. The field data, and some integrals obtained from them, were examined in order to assess the impact of the number of lobes. Finally, thrust loss and mass flow rates that allowed an examination of thrust coefficient variation were measured. The reduction in the measured thrust coefficient was compared with estimates of the penalty utilizing boundary-layer data. These results are summarized in the following.

II. Experimental Procedure

The data were obtained in an open jet facility. Compressed air passed through a cylindrical plenum chamber fitted with flow conditioning units and then through the nozzle to discharge into the quiescent ambient. The experiments involved "cold" flow, that is, the jet was unheated and the total temperature was approximately the same throughout and equaled that in the ambient. Data from four nozzles are to be presented. All have convergent interiors with approximately 0.64-cm-long constant cross-section passage prior to the exit. The inlet is circular with 3.81-cm diam, and the convergence to exit shape takes place over an axial distance of 7.62 cm. The equivalent diameter D based on the exit area A is 1.47 cm for all four cases. One of the four nozzles having circular geometry represents the baseline case. The rest are of lobed configurations, having 6, 10, and 14 lobes. The exit geometry (for the 10-lobed case) is shown schematically in Fig. 1, and the relevant dimensions for all cases are listed in Table 1. The second-to-last column shows the ratio of "wetted" perimeter to equivalent diameter of the nozzle

Received 11 June 2002; revision received 8 October 2002; accepted for publication 18 November 2002.

*Aerospace Engineer, Turbomachinery and Propulsion Systems Division. Associate Fellow AIAA.

†National Research Council Associate; currently Aerospace Engineer, John A. Volpe Center, U.S. Department of Transportation, Cambridge, MA 02142. Senior Member AIAA.

‡Aerospace Engineer, Turbomachinery and Propulsion Systems Division. Senior Member AIAA.

Table 1 Lobed nozzle geometry (dimensions are in centimeters)

Nozzle	W	H	a	b	P/D	$H/(a+b)$
Round	——	——	——	——	π	——
6-lobe	2.240	1.400	0.310	0.658	2.52π	1.45
10-lobe	2.240	1.400	0.208	0.300	3.63π	2.76
14-lobe	2.240	1.400	0.155	0.193	4.80π	4.02

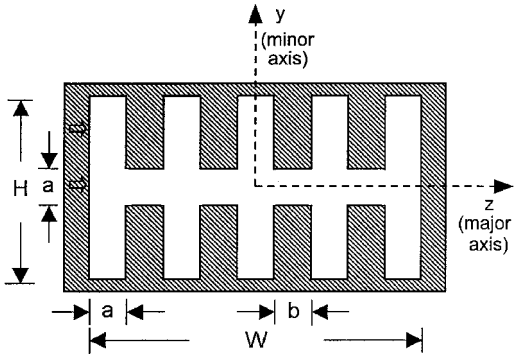

Fig. 1 Schematic of exit geometry of 10-lobed nozzle.

exit, which is a measure of perimeter stretching caused by the lobes. The last column shows the lobe-height-to-wavelength ratio that is sometimes used to specify the lobe geometry.[6,7]

Standard procedures were followed for far-field noise measurement using a $\frac{1}{4}$-in. microphone (B&K). Even though the laboratory was not anechoic, sufficient acoustic absorbent materials were used on and around the facility so that the noise data did not suffer from any significant contamination. The validity of the data was checked earlier[1] by comparing the noise spectra with data available from the literature. The measurement location was $63D$ from the jet exit. Spectral analysis was done with a 400-line analyzer (Nicolet). Noise data were obtained at two angles α relative to the jet axis. An orifice meter mounted on the supply line measured mass flow rate. Thrust was measured by a one-component force balance; further details can be found in earlier publications.[16,17] Repeatability of the noise spectral amplitudes was within 0.5 dB. Uncertainty in the thrust data was within 1%.

As stated in the Introduction, the acoustic data were obtained for a nominal jet Mach number of 0.94. At this Mach number hot-wire data were obtained only on the jet axis as a result of probe breakage and other difficulties. More frequent probe breakage was encountered during attempts to measure the exit boundary layer. The boundary-layer measurement was carried out at $x \approx 0.25$ mm. There, high shear and possible freezing of moisture from entrained ambient air were likely responsible for the low probe survivability. Furthermore, the boundary layer could be measured only on one side, having the probe inserted at an angle, so that only the sensor and a small part of the prongs were in the flow. Thus, with the lobed nozzles these measurements were not done for the inner lobes. The boundary-layer data were acquired up to a Mach number of about 0.65. A detailed survey of the three-dimensional flowfield was conducted at a jet Mach number of 0.30. The measurement at the lower Mach number was unambiguous, free from sensor survivability problems, and inexpensive because the lower supply pressure could be furnished with an auxiliary blower. The independent operation with the blower allowed sustained runs over long periods that were necessary for the surveys. Whereas the velocity and turbulence data at the lower Mach number represent the streamwise components, the data at the higher Mach number are qualitative. A relatively high overheat ratio was used in constant-temperature mode so that the hot wire essentially responded to mass flux (velocity times density). Limited data were also obtained at the higher Mach number using particle image velocimetry (PIV); the procedure will be briefly described with the data.

III. Results

A. Noise Field

Figure 2a shows sound-pressure spectra, at $\alpha = 90$ deg, for the three lobed cases compared to the baseline circular case. For these

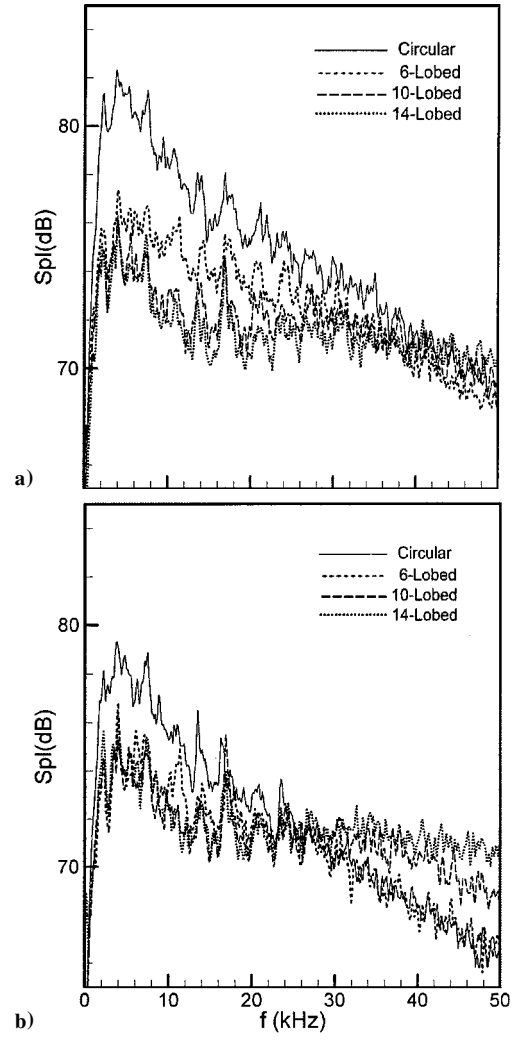

Fig. 2 Sound-pressure spectra at α = 90 deg, on minor axis, for indicated nozzles: a) constant pressure ratio, M_j = 0.94 and b) constant thrust, $T \approx$ 17 N.

data the supply pressure is held constant; thus, the jet Mach number is the same for all cases. It is apparent that the noise is low for all lobed cases. Increasing the number of lobes from 6 to 10 produces some additional noise benefit. However, there is only marginal gain with further increase in the number of lobes to 14. Figure 2b shows spectra for the same cases of Fig. 2a except that the thrust is held constant. (Thrust for the 14-lobed nozzle is the same between the two figures.) A similar conclusion is reached regarding the influence of number of lobes. However, it can be seen that the high-frequency noise for the 10- and 14-lobed cases is relatively high. The implication of this is discussed shortly. Corresponding noise spectra at $\alpha = 25$ deg for constant Mach number are shown in Fig. 3a, and for constant thrust are shown in Fig. 3b. Again, a similar observation can be made regarding the effect of number of lobes.

The spectra in Figs. 2 and 3 are obtained on the minor axis plane. Corresponding data obtained on the major axis plane are compared for the six-lobed nozzle, as an example, in Fig. 4. At $\alpha = 90$ deg in Fig. 4a, there is practically no difference in the spectra between the minor and the major axis planes. This demonstrates the axisymmetry of the noise field,[1] even though the flowfield is quite asymmetric initially. At $\alpha = 25$ deg the amplitudes are identical at lower frequencies; however, high-frequency amplitudes are higher on the minor axis plane. Data for minor axis plane are compared in Figs. 2 and 3; thus, the inferred noise benefits are conservative.

The overall sound-pressure levels, obtained by integration of the spectral data of Figs. 2 and 3, are shown in Fig. 5a. The data are shown as a function of number of lobes, with the circular jet data shown at an abscissa value of unity. The amplitudes decrease with

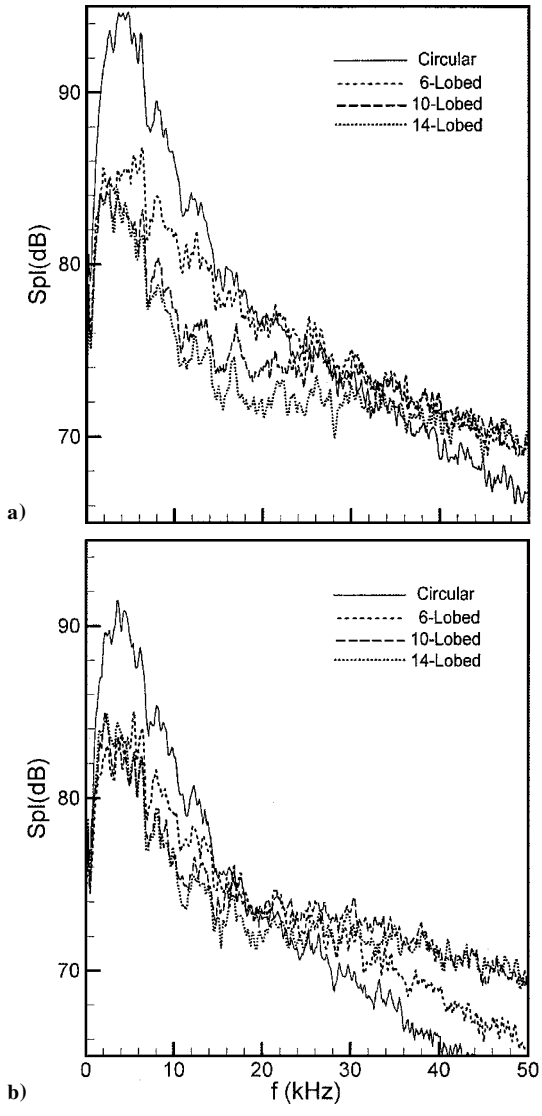

Fig. 3 Sound-pressure spectra at α = 25 deg, on minor axis, for indicated nozzles: a) constant pressure ratio, M_j = 0.94 and b) constant thrust, $T \approx 17$ N.

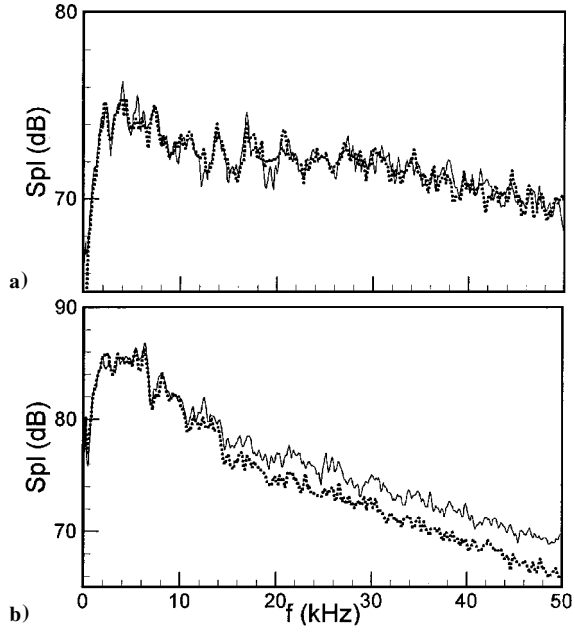

Fig. 4 Sound-pressure spectra for six-lobed nozzle at M_j = 0.94: ——, minor axis; · · · ·, major axis. a) α = 90 deg and b) α = 25 deg.

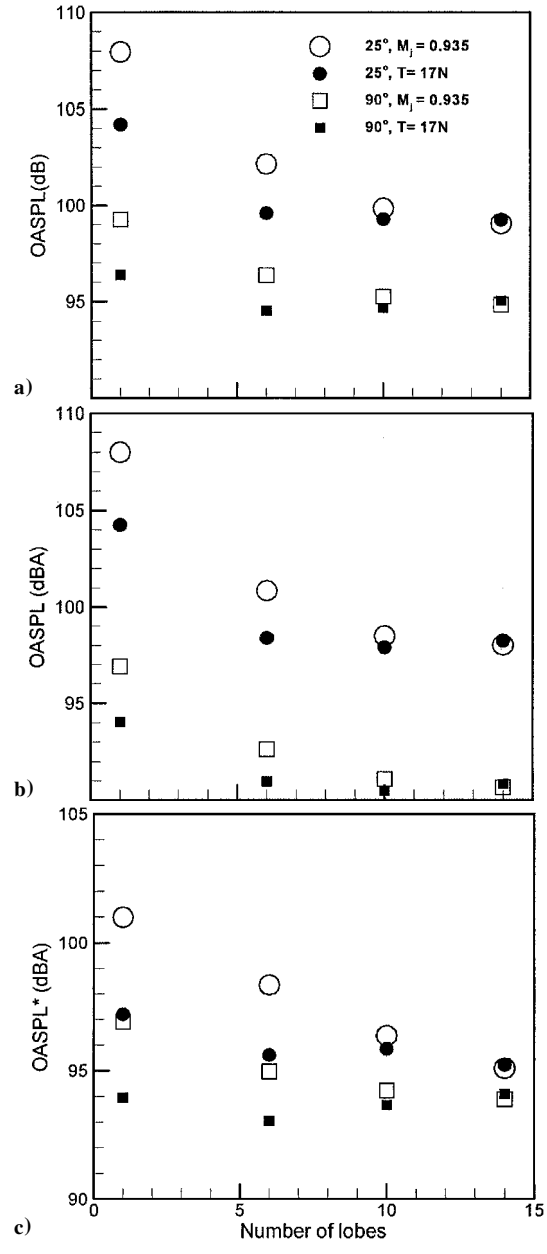

Fig. 5 Overall sound-pressure level (OASPL) corresponding to the data of Figs. 2 and 3, shown as a function of number of lobes: a) OASPL, b) A-weighted OASPL, and c) A-weighted OASPL after scaling by a factor of 20.

increasing number of lobes, for both values of θ and for both cases of constant Mach number and constant thrust. However, the increased high-frequency noise can weigh in differently in perceived noise levels.[18] Here, A-weighted noise levels were calculated to assess this, and the results are shown in Fig. 5b. The levels are somewhat different, but the trend remains the same as seen in Fig. 5a. Furthermore, in order to simulate the noise from a realistic practical nozzle the spectra data were scaled by a factor of 20, that is, assuming a Strouhal-number scaling, the frequencies were divided by 20 to simulate noise from a 20 times larger nozzle. The data were then integrated to obtain the A-weighted (dBA) levels. The results are shown in Fig. 5c. It is apparent that, after these considerations, the noise benefit is not as attractive as it first appeared. Nevertheless, a net noise reduction with the six-lobed nozzle is evident for all conditions. Further reduction with a greater number of lobes appears marginal or even questionable.

B. Flowfield

First, the exit boundary-layer data are shown in Fig. 6. Momentum thickness variation with Reynolds number is shown; a scale

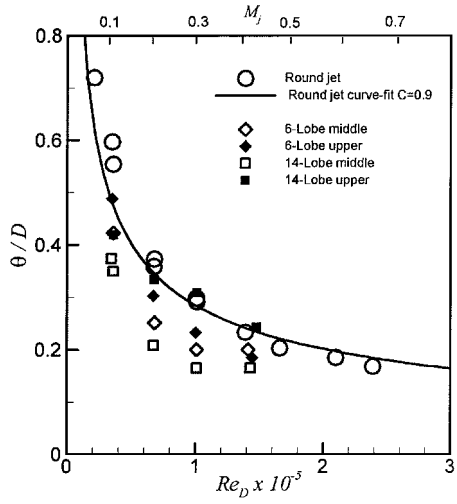

Fig. 6 Boundary-layer momentum thickness vs Reynolds number.

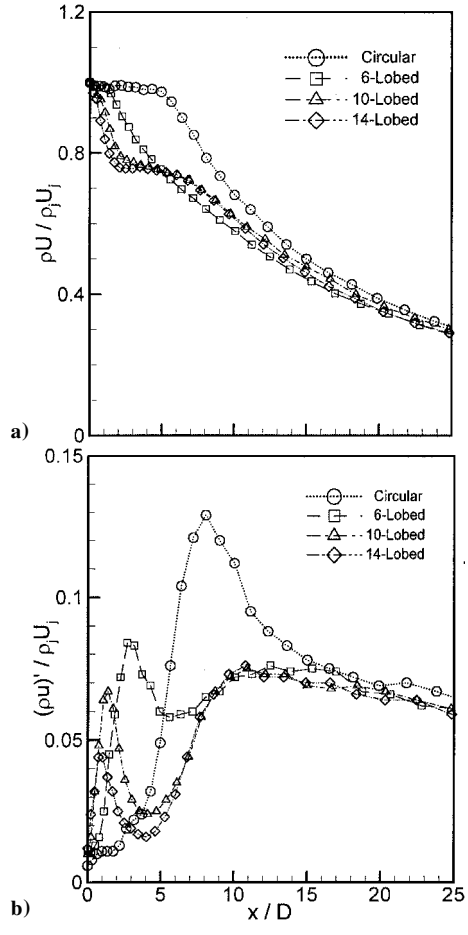

Fig. 7 Hot-wire results for centerline profiles at M_j = 0.94: a) mean and b) turbulence intensity.

for corresponding Mach number is displayed at the top for easy reference. These data could be obtained only for relatively low subsonic conditions as a result of frequent probe breakage (Sec. II). Also, in this and some other sets of measurement the 10-lobed nozzle was excluded, and data for the circular, 6-, and 14-lobed cases were deemed sufficient. With the lobed nozzles the boundary layer was measured at two locations, indicated with the small arrows in Fig. 1. It is found that the circular nozzle data follow the equation $\theta/D = C/\sqrt{(Re_D)}$, where Re_D is the Reynolds number based on the diameter D. The constant $C = 0.9$, yielding best fit through the data, is comparable to that found in many previous studies.[19] Based on the functional dependence of θ on Re_D, the boundary layer is inferred to be nominally laminar (nominal because fluctuation intensity within the boundary layer is high). For the lobed nozzles the momentum thicknesses are somewhat smaller than that found for the round nozzle. However, the values are comparable, and again a nominally laminar state is inferred. Peak velocity fluctutation intensity u'/U_j within the boundary layer at $M_j = 0.3$ was measured to be about 0.03, 0.04, and 0.08 for the circular, 6-lobe and 14-lobe cases, respectively; here, U_j is the jet velocity corresponding to the Mach number M_j. The turbulence is higher for the 14-lobed case; however, this is not unusual with nominally laminar state.[18,19] Furthermore, from a smooth variation of thrust, to be discussed in Sec. III.C, the boundary layer was inferred to remain nominally laminar for all of the cases even at $M_j = 0.94$.

Centerline variations of mean velocity and turbulence intensity are shown in Figs. 7a and 7b for $M_j = 0.94$. As stated in Sec. II, the hot-wire data are approximations of mass flux ρu rather than velocity u. A faster decay of the mean value is observed for the lobed nozzles, indicating a faster jet spreading. Corresponding turbulence data (Fig. 7b) show that a peak occurs close to the nozzle and that the location of this peak shifts upstream with a greater number of lobes. There occurs a second, less pronounced, peak around $x/D = 12$. The second peak for any of the lobed cases is found to be of much smaller amplitude compared to the peak for the circular case. The flowfield, approximately 6–12 diameters from the nozzle, has been identified as the source region for jet noise in various studies.[20] Thus, a lower turbulence in the noise-producing region is commensurate with the lower far-field noise for the lobed cases (Figs. 2–5).

Detailed flowfield measurement at $M_j = 0.94$ was attempted using the PIV technique. A Thermo-Systems, Inc., instrument package was used for the measurement. The flow in the plenum chamber was seeded with olive-oil-based fog particles. Mean and rms velocity fields were measured based on averages over 56 frames. An algorithm after Scarano and Riethmuller [21] was used in the data reduction. However, because of drifts in seeding, laser system, and alignment of optics, good data repeatability could not be ensured. The results, considered qualitative, for only the circular and the 14-lobed nozzles are shown in Figs. 8 and 9. The mean velocity fields for the two nozzles are compared in Fig. 8, and the turbulence intensity fields are compared in Fig. 9. The turbulence results confirm the occurrence of a high-intensity region close to the lobed nozzle, observed earlier with the hot-wire data (Fig. 7b). The flowfields in Figs. 8 and 9 extend up to about $x/D = 4.5$. Thus, the second high intensity region of Fig. 7b is not captured. It should be apparent that

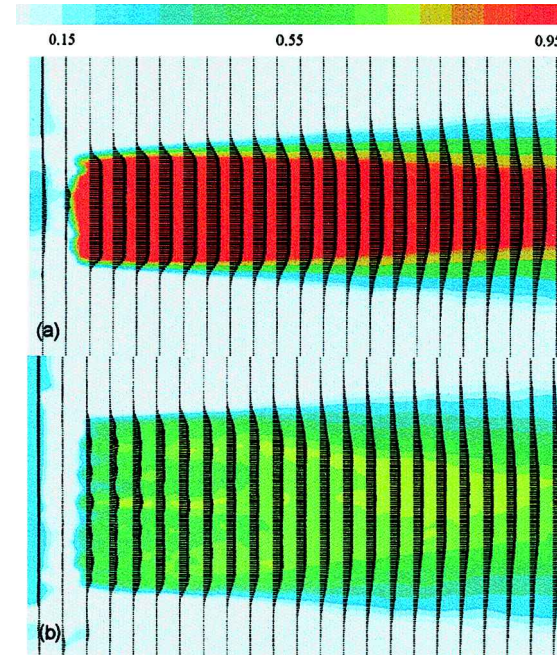

Fig. 8 Mean velocity field on major-axis plane (DPIV data): a) circular and b) 14-lobed nozzles; $M_j \approx 0.94$.

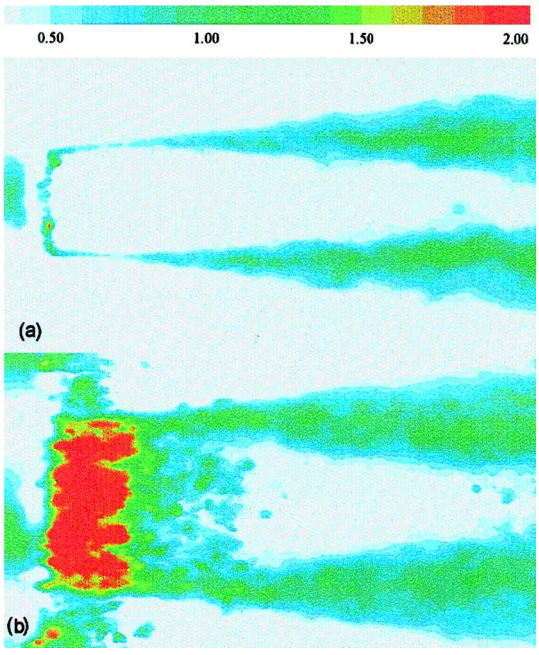

Fig. 9 Turbulence intensity field on major-axis plane corresponding to the cases of Fig. 8.

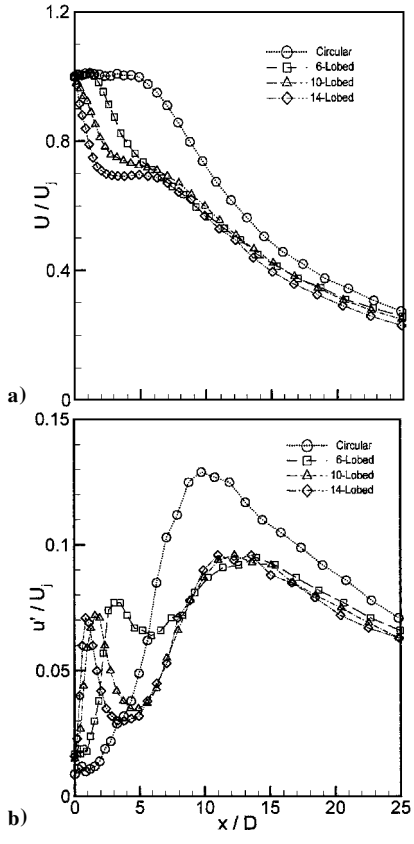

Fig. 10 Centerline profiles at $M_j = 0.30$: a) mean velocity and b) turbulence intensity.

the second peak, on the jet axis, takes place following the merger of the outer shear layers. The occurrence of the first peak close to the nozzle is somewhat intriguing, and this is further explored with hot-wire anemometry.

Because the hot-wire technique is inherently difficult and subject to question in compressible flows, the measurements are repeated at a low jet Mach number (0.3). Corresponding centerline variations of U and u' are shown in Fig. 10, in a similar manner as in Fig. 7. The trends appear essentially the same as seen in Fig. 7. This result encouraged further exploration at the lower Mach number with the expectation that the overall flowfields are also similar at the two Mach numbers. As stated in Sec. II, detailed surveys could be carried out at the lower M_j with confidence and relative ease. An examination of the entire flowfield was deemed important because centerline data especially for a nonaxisymmetric case cannot fully represent the jet evolution.

First, surveys were conducted on a quadrant of the cross section for only the 14-lobed nozzle. The surveys, involving as much as 36×20 grid points, were done at several x stations. Mean velocity distributionsare shown in Fig. 11. Note that an enlarged scale is used to show the data at the upstream measurement locations ($x/D \leq 1$). Also, for easy reference the outline of the nozzle exit is overlaid with white lines. The cellular structure in the distributions, because of the lobes, can be seen in the upstream regions. By the last station $x/D = 7$ the jet cross section has become almost round.

The corresponding turbulence intensity distributions are shown in Fig. 12. Again, an enlarged spatial scale is used for the data at the upstream locations. First, from the data farther downstream ($x/D \geq 2$) one can see the spreading of the outer shear layer. High turbulence from the shear layer spreads with increasing distance and, by $x/D = 7$, has almost engulfed the core of the jet. At the upstream locations (left column) the turbulence is also high in the outer shear layer, as high as about 0.13. However, the color legend has been chosen to show levels only up to 0.08. Thus, red represents a level of 0.08 or higher. This is done in order to show clearly the distributions within the core of the jet where the levels are relatively lower. One can now see the evolution of high turbulence intensity within the core at locations close to the nozzle. After the turbulence has spread over most of the cross section around $x/D = 0.75$, a subsequent "quenching" of turbulence can also be clearly seen. It is apparent that the initial high turbulence occurs because of the interaction and spreading of the shear layers shed from the lobes. The turbulence then decays, similarly as in the flow behind a turbulence-generating grid. Meanwhile, the turbulence is high in the outer shear layer that separates the jet from the ambient fluid. It is also clear that the second peak in the centerline u' profile occurs following the convergence of the outer shear layer on the axis. This takes place downstream of the last station covered in Fig. 12.

If one assumes that the first peak occurs upon the merger of the shear layers shed from an individual lobe, it follows that the distance of the location of the first peak scales on the width of the lobes. Thus, the first peak should occur closer to the nozzle with smaller lobes. This is indeed the case in both Figs. 7 and 10. With reference to the data of Table 1, the first peak is found to occur in the x/a range of 4–6.

A complete description of the flowfields would require detailed data as in Figs. 11 and 12 over the entire cross section at many x stations. Carrying this out for all of the nozzles was deemed formidable. Thus, in an attempt to compare and quantify the flowfield evolution only radial profiles were acquired at several x stations covering the developing regions of the jets. For the lobed cases two profiles were obtained: one on the major axis and the other on the minor axis.

Mean velocity profiles are shown in Fig. 13. The evolution of the flowfield until reaching an asymptotic state can be observed. The profiles at the farthest x/D have become almost congruent. Close to the nozzle an inspection of the data for the 14-lobed case reveals similarity between Figs. 8b and 13a. The "wavy" profiles match well. This agreement reinforces the notion that the three-dimensional flowfields at the low and high Mach numbers are essentially similar. Turbulence intensity profiles corresponding to the cases of Fig. 13 are not presented here in order to conserve space. A computational fluid dynamics (CFD) effort is currently underway[22] for assessing the applicability of different turbulence models for successful prediction of the present results. So far, the occurrence of the first turbulence peak has not been captured well, and this is under further investigation. The turbulence profiles will be presented together with the CFD results in the conference paper.[22]

To compare the overall impact on the flowfields, the mean velocity and the turbulence intensity profiles were integrated. Two integrals,

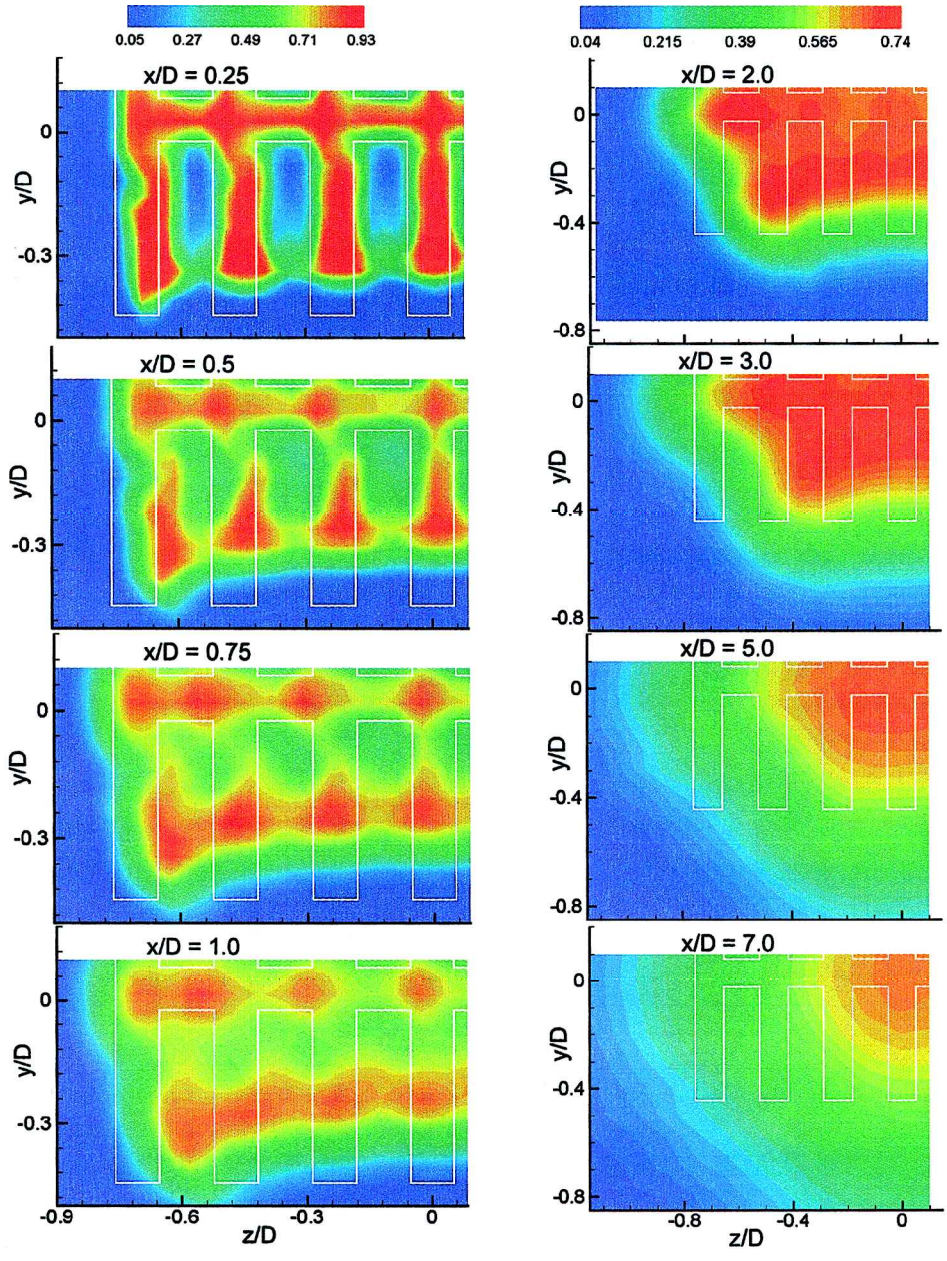

Fig. 11 Cross-sectional distributions of mean velocity for the 14-lobed nozzle at indicated x/D: $M_j = 0.3$ (hot-wire data).

axial volume flow rate $\dot{Q}$, and turbulent momentum flux k^*, were calculated as follows:

$$\dot{Q} = 2\pi \int rU \, dr \tag{1}$$

$$k^* = 2\pi \int ru'^2 \, dr \tag{2}$$

The integrals were normalized by the respective initial values $(\dot{Q}_e =) A_e U_j$ and $(K_e =) A_e U_j^2$, where A_e is the equivalent area of the nozzle exit. The flow blockage for individual nozzles was taken into account in calculating A_e before data normalization. (See mass flow rate data in Sec. III.C.)

For the circular jet the integration was performed from the centerline in both positive and negative r direction, and an average of the two integrals was taken. For the lobed cases similar integrals were obtained for each of the major and minor axis planes. An average of the four integrals was then taken for each lobed case. It can be shown that such an average would be representative of the respective integral if the contours on the cross-sectional plane were elliptic in shape. This is a reasonable approximation for the lobed cases only after a distance of a few diameters from the exit. Thus, data close to the nozzle for the lobed cases are omitted in the following figures.

Streamwise variations of $\dot{Q}$ are shown in Fig. 14a. The data for the circular nozzle can be compared with published results. The magnitudes ($\dot{Q}/\dot{Q}_e = 3.6$ at $x/D = 14$) and the slope (entrainment rate, about 0.26) agree reasonably with published data.[17] For either lobed case the magnitudes are higher, indicating a faster jet spreading. However, the increase in $\dot{Q}$, say at $x/D = 14$ by about 20% relative to the circular nozzle data, is rather modest. Larger increases have been achieved when using other mixing enhancement techniques.[17] Those other techniques (e.g., vortex generators or periodic forcing at the "preferred mode"), however, involve an increase in the turbulence intensities over most of the developing region of the jet. Here, the turbulence is high only close to the nozzle, but subsequently it is remarkably low even as the jet evolves to reach the asymptotic state. The comparison based on the integral k^* confirms that the turbulence is low not only on the centerline but also overall on an integral basis. These data are shown in Fig. 14b. It can be seen that for $x/D > 6$ the integrated turbulent momentum flux k^* is indeed consistently low for the lobed cases.

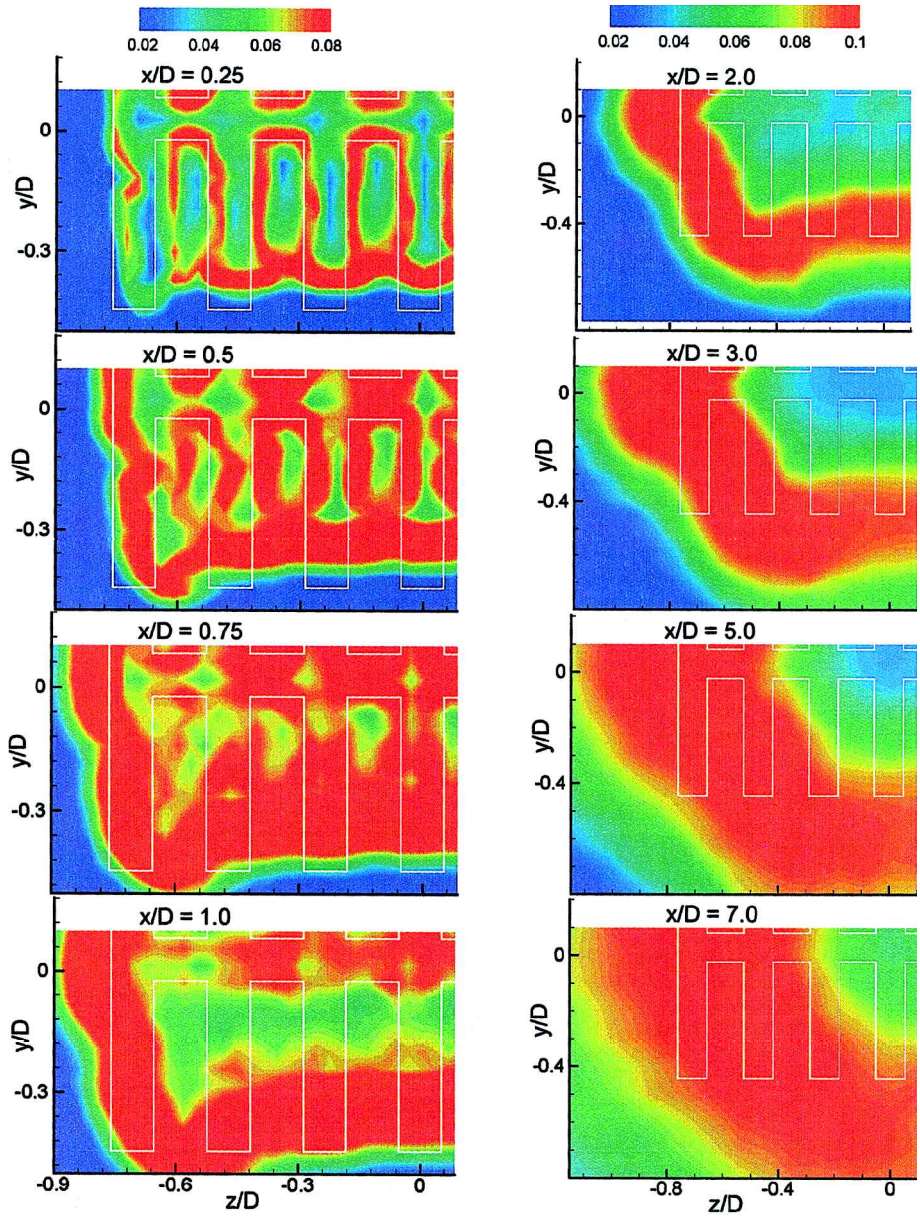

Fig. 12 Turbulence intensity distributions corresponding to cases of Fig. 11; indicated *x/D*: $M_j = 0.3$.

C. Thrust Loss

Thrust and mass flow rate data for the four nozzles are shown in Figs. 15a and 15b, respectively, as a function of jet Mach number. Here, the measurements are extended to supersonic regime, where the flow is underexpanded. M_j in the latter regime represents the fully expanded Mach number, that is, Mach number had the flow expanded fully. The solid lines in these figures represent ideal values (assuming a top-hat exit velocity profile with zero boundary-layer thickness). Data for the circular and six-lobed cases are barely distinguishable from the ideal curves. However, there is noticeable thrust loss and flow blockage for the 10- and 14-lobed nozzles. Referring back to earlier discussion in Sec. III.B one also notes that the curves in both figures are smooth and, thus, the initial boundary layers must not have gone through transition to a turbulent state. Had transition occurred, a departure from the smooth variation should have taken place.

Thrust coefficient, calculated from the data of Figs. 15a and 15b, are shown in Fig. 15c. It is essentially unity within measurement uncertainty (Sec. II), for the circular nozzle. It is clearly but only slightly lower for the six-lobed case. At $M_j = 0.94$ about 7-dBA noise reduction (Fig. 5b, $\alpha = 25$-deg case; open circles) has been achieved while C_f dropped to 0.982. With increasing number of lobes, C_f becomes significantly lower than unity.

With a lobed nozzle the larger wetted perimeter involves a larger amount of boundary-layer fluid having lower momentum. Thus, a stretching of the perimeter with increased number of lobes is expected to result in more thrust loss as long as the boundary-layer thickness remains approximately the same. It is possible to estimate this loss from the boundary-layer measurement. This estimate is valid when all lobes have at least some core region of uniform flow and the boundary-layer thickness δ is smaller than the smallest lobe dimension ($\delta < a/2$; see Fig. 1). For such a flow the thrust deficit (ΔT) per unit perimeter caused by viscous losses from the boundary layer is

$$\Delta T = \int_0^\delta \left(\rho_j U_j^2 - \rho U^2\right) \mathrm{d}y \tag{3}$$

This can be related to the displacement δ^* and momentum θ thicknesses, given by

$$\delta^* = \int_0^\delta \left(1 - \frac{\rho U}{\rho_j U_j}\right) \mathrm{d}y \tag{4}$$

$$\theta = \int_0^\delta \frac{\rho U}{\rho_j U_j}\left(1 - \frac{U}{U_j}\right) \mathrm{d}y \tag{5}$$

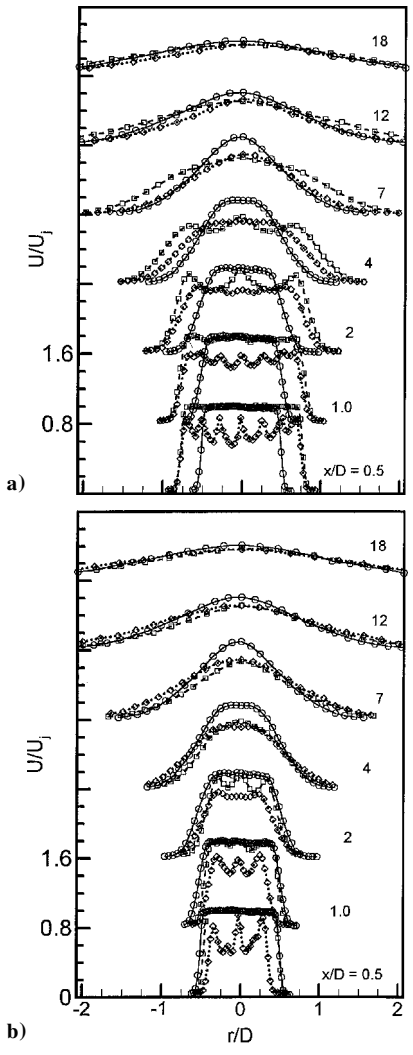

Fig. 13 Cross-sectional profiles of axial mean velocity for these nozzles: ○, circular; □, 6-lobe; and ◇, 14-lobe. M_j = 0.30: a) major axis and b) minor axis. Successive sets of profiles staggered by one major division.

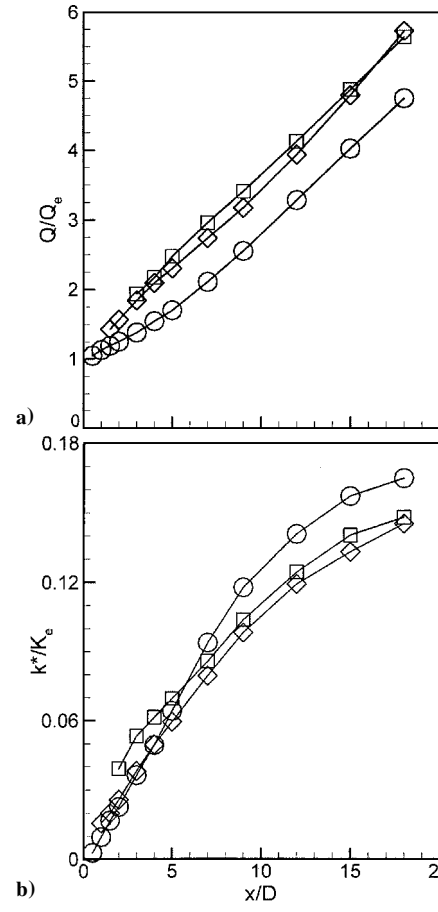

Fig. 14 Streamwise variation of integrated quantities: a) volume flow rate and b) turbulent momentum flux: ○, circular nozzles; □, 6-lobe nozzles; and ◇, 14-lobe nozzles: M_j = 0.30.

Multiplying Eqs. (4) and (5) by $\rho_j U_j^2$ and adding, one obtains

$$\rho_j U_j^2(\delta^* + \theta) = \int_0^\delta \left(\rho_j U_j^2 - \rho U^2\right) \mathrm{d}y \tag{6}$$

Comparing with Eq. (3) it follows that the quantity $\rho_j U_j^2(\delta^* + \theta)$ is equal to the thrust deficit per unit perimeter. In analogy to the significance of displacement thickness δ^* for mass flow rate, the thickness $\delta^* + \theta$ has the same significance for thrust. That is, the latter thickness with a uniform flow having the freestream velocity would account for the thrust loss caused by the boundary layer.

The thrust coefficient can be expressed as

$$C_f = \frac{\text{ideal thrust} - \text{thrust deficit}}{\text{ideal thrust}}$$

where the ideal thrust is $\rho_j U_j^2 A$ and A is the nozzle exit area. With P being the perimeter at the nozzle exit, it follows that

$$C_f = \frac{\rho_j U_j^2 A - \rho_j U_j^2(\delta^* + \theta)P}{\rho_j U_j^2 A}$$

which simplifies to

$$C_f = 1 - (\delta^* + \theta)(P/A)$$

Substituting the equivalent diameter, this can be written as

$$C_f = 1 - 4[(\delta^* + \theta)/D](P/\pi D) \tag{7}$$

Equation (7) can be rearranged to relate the loss in thrust coeffiecient $(1 - C_f)$ to the perimeter stretching factor P/D and the boundary-layer thicknesses. Note that the latter are inversely proportional to the square root of the Reynolds number Re_D. Referring back to Fig. 6, first one notes that the boundary-layer thickness compared to the lobe width is indeed small even for the 14-lobed case. (With $\theta/D \approx 0.002$, δ/D is estimated to be 0.015, so that $a/2\delta \approx 3.5$.) Thus, the thrust estimate ought to be reasonable even for the 14-lobed nozzle. The thickness data measured for the circular nozzle at $M_j = 0.66$ were $\theta/D \approx 0.0017$ and $\delta^*/D = 0.0036$. If we assume these to be representative of all of the nozzles at that Mach number and take the P/D data from Table 1, the estimated thrust coefficient turns out to be 0.98, 0.95, 0.92, and 0.90 for the circular, 6-lobe, 10-lobe, and 14-lobe nozzles, respectively.

Inspecting Fig. 15c, it is found that the measured thrust coefficients around $M_j = 0.66$ are not far from the estimated values. One then infers that the lower momentum fluid in the extended boundary layer over the stretched perimeter essentially accounts for most of the thrust loss. There are other sources of thrust loss, for example, caused by secondary flow at the corners of the lobes, base drag at the lips of the lobes, etc. However, the estimates imply that the deficit is dominated by viscous losses caused by the boundary layer and other factors are less important, for the geometry under consideration. Finally, for the given nozzles the loss in thrust coefficient is quite drastic with the increasing number of lobes. However, with a larger size nozzle having same geometry and number of lobes the loss in C_f should be less because the Reynolds number would be higher. An alleviation in the loss with increasing Re_D can be inferred from Eq. (7), as stated earlier. The trend is also borne out by the data in Fig. 15c. For a given nozzle Eq. (7) would allow an estimate of the expected thrust loss if data or estimate of the boundary-layer thicknesses were available.

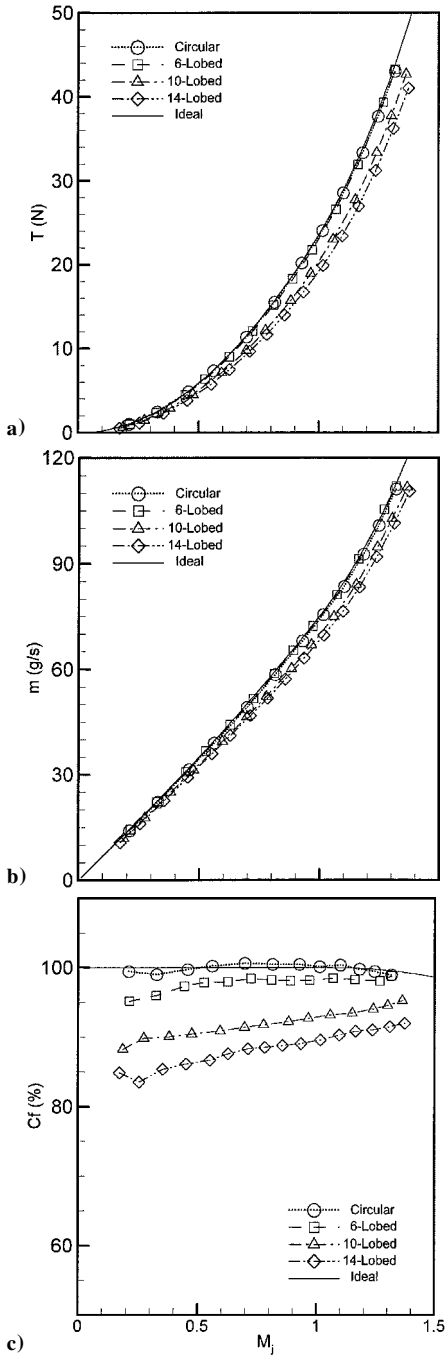

Fig. 15 Thrust and mass flow rate vs M_j for indicated nozzles: a) thrust, b) mass flow rate, and c) thrust coefficient.

IV. Conclusions

Flow and noise fields of lobed nozzles are studied in this paper. The effect of number of lobes for a fixed exit area of the nozzle is considered. All lobed nozzles involve a mildly faster spreading of the jet compared to the circular case. On the centerline of the jet, the turbulence intensity exhibits a peak close to the nozzle followed by a second peak farther downstream. It is inferred that the first peak occurs when the shear layers from the lobes merge together. The distance of the location of the first peak, thus, scales as the width of the lobes. In comparison, the second peak occurs approximately 12 jet diameters downstream. The latter peak occurs after the outer shear layers converge on the jet axis. The corresponding profile for the circular jet is characterized by only the second peak, 8–10 diameters downstream. From somewhat downstream of the first peak, the turbulence intensities are significantly lower with the lobed nozzles compared to the intensities in the circular case. This is true not only on the centerline but also overall as reflected by the turbulent momentum flux obtained by integration of the data over the cross section.

Increasing the number of lobes results in a progressive reduction in the turbulence intensities as well as overall noise. However, this also involves a progressive reduction in the thrust coefficient. The measured thrust loss is shown to be primarily caused by increased amount of low-momentum boundary-layer fluid over the stretched perimeter. Among the cases studied, the six-lobed nozzle has the optimum reduction in turbulence and noise with minimal thrust penalty. It is possible that the optimum number of lobes could be larger for a larger size nozzle because an increase in Reynolds number would alleviate the thrust loss. It is also clear that, for a given size of the nozzle, a certain (moderate) number of lobes is optimum, and further increase in the number produces a diminishing return in noise benefit while rapidly increasing the thrust penalty. The lobed geometry becomes detrimental for thrust when the boundary-layer thickness is a significant fraction of the lobe width. Noting that for the six-lobed nozzle $C_f \approx 0.98$ while $a/2\delta \approx 7.5$, a guideline for choosing the lobe dimension (and hence number of lobes) could be that the lobe width be an order of magnitude larger than the boundary-layer thickness.

Acknowledgment

This work is supported by the Aerospace Propulsion and Power Research and Technology Base Program at NASA John H. Glenn Research Center.

References

[1]Tam, C. K. W., and Zaman, K. B. M. Q., "Subsonic Jet Noise from Nonaxisymmetric and Tabbed Nozzles," *AIAA Journal*, Vol. 38, No. 4, 2000, pp. 592–599.

[2]Zaman, K. B. M. Q., and Tam, C. K. W., "Flow and Noise Field of Subsonic Jets from Asymmetric Nozzles," AIAA Paper 99-3583, June 1999.

[3]Panda, J., and Zaman, K. B. M. Q., "Density Fluctuation in Asymmetric Nozzle Plumes and Correlation with Far-Field Noise," AIAA Paper 2001-0378, Jan. 2001.

[4]McCormick, D. C., and Bennett, J. C., "Vortical and Turbulent Structure of a Lobed Forced Mixer Free-Shear Layer," *AIAA Journal*, Vol. 32, No. 9, 1994, pp. 1852–1859.

[5]Yu, S. C. M., and Yip, T. H., "Measurements of Velocities in the near Field of a Lobed Forced Mixer Trailing Edge," *Aeronautical Journal*, Vol. 101, March 1997, pp. 121–129.

[6]Abolfadl, M. A., Metwally, M. A., El-Messiry, A. M., and Ali, M. A., "Experimental Investigation of Lobed Mixer Performance," *Journal of Propulsion and Power*, Vol. 17, No. 5, 2001, pp. 1109–1116.

[7]Elliott, J. K., Manning, T. A., Qui, Y. J., Greitzer, E. M., Tan, C. S., and Tillman, T. G., "Computational and Experimental Studies of Flow in Multi-Lobed Mixers," AIAA Paper 92-3568, July 1992.

[8]Waitz, I. A., Greitzer, E. M., and Tan, C. S., "Vortices in Aero-Propulsion Systems," *Fluid Vortices*, edited by S. I. Green, Kluwer Academic, Norwell, MA, 1995, pp. 471–532.

[9]Longmire, E. K., Eaton, J. K., and Elkins, C. J., "Control of Jet Structure by Crown-Shaped Nozzles," *AIAA Journal*, Vol. 30, No. 2, 1992, pp. 505–512.

[10]Lasheras, J., and Prestridge, K., "Three-Dimensional Vorticity Dynamics in Coflowing Jets Subjected to Axial and Azimuthal Forcing," AIAA Paper 97-1880, June–July 1997.

[11]Samimy, M., Kim, J. -H., Clancy, P. S., and Martens, S., "Passive Control of Supersonic Rectangular Jets via Nozzle Trailing-Edge Modifications," *AIAA Journal*, Vol. 36, No. 7, 1998, p. 1230.

[12]Kim, J. -H., and Samimy, M., "Mixing Enhancement via Nozzle Trailing Edge Modifications in a High Speed Rectangular Jet," *Physics of Fluids*, Vol. 11, No. 9, 1999, pp. 2731–2742.

[13]Gilinsky, M. M., and Seiner, J. M., "Corrugated Nozzles for Acoustic and Thrust Benefits," AIAA Paper 96-1670, May 1996.

[14]Hu, H., Kobayashi, T., Saga, T., Taniguchi, N., Liu, H., and Wu, S., "Research on the Rectangular Lobed Exhaust Ejector/Mixer Systems," *Transactions of the Japan Society of Aeronautics and Space Science*, Vol. 41, No. 134, 1999, pp. 187–194.

[15]Hu, H., Kobayashi, T., Saga, T., Segawa, S., and Taniguchi, N., "Particle Image Velocimetry and Planar Laser-Induced Fluorescence Measurements on Lobed Jet Mixing Flows," *Experiments in Fluids*, Supplemental Issue, Springer-Verlag, 2000, pp. S141–S157.

[16]Zaman, K. B. M. Q., Reeder, M. F., and Samimy, M., "Control of an Axisymmetric Jet Using Vortex Generators," *Physics of Fluids A*, Vol. 6, No. 2, 1994, pp. 778–793.

[17]Zaman, K. B. M. Q., "Spreading Characteristics of Compressible Jets from Nozzles of Various Geometries," *Journal of Fluid Mechanics*, Vol. 383, 1999, pp. 197–228.

[18]Simonich, J. C., Narayanan, S., Barber, T. J., and Nishimura, M., "Aeroacoustic Characterization, Noise Reduction, and Dimensional Scaling Effects of High Subsonic Jets," *AIAA Journal*, Vol. 39, No. 11, 2001, pp. 2062–2069.

[19]Hussain, A. K. M. F., and Zedan, M. F., "Effects of the Initial Condition on the Axisymmetric Free Shear Layer: Effect of the Initial Fluctuation Level," *Physics of Fluids*, Vol. 21, No. 9, 1978, pp. 1475–1481.

[20]Fisher, M. J., Harper-Bourne, M., and Glegg, S. A. L., "Jet Noise Source Location: the Polar Correlation Technique," *Journal of Sound and Vibration*, Vol. 5, No. 1, 1977.

[21]Scarano, F., and Riethmuller, M. L., "Advances in Iterative Multigrid PIV Image Processing," *Experiments in Fluids*, Supplemental Issue, Springer-Verlag, 2000, pp. S51–S60.

[22]Georgiadis, N. J., Rumsey, C. L., Yoder, D. A., and Zaman, K. B. M. Q., "Effects of RANS Turbulence Modeling on Calculation of Lobed Nozzle Flowfields," AIAA Paper 2003-1271, Jan. 2003.

W. J. Devenport
Associate Editor